UCRL- 90819
PREPRINT

A NUMERICAL STUDY OF NONSPHERICAL BLACK HOLE ACCRETION

John F. Hawley and Larry L. Smarr
Department of Astronomy, University of Illinois

James R. Wilson
Lawrence Livermore National Laboratory

THIS PAPER WAS PREPARED FOR SUBMITTAL TO
THE ASTROPHYSICAL JOURNAL
February 1984

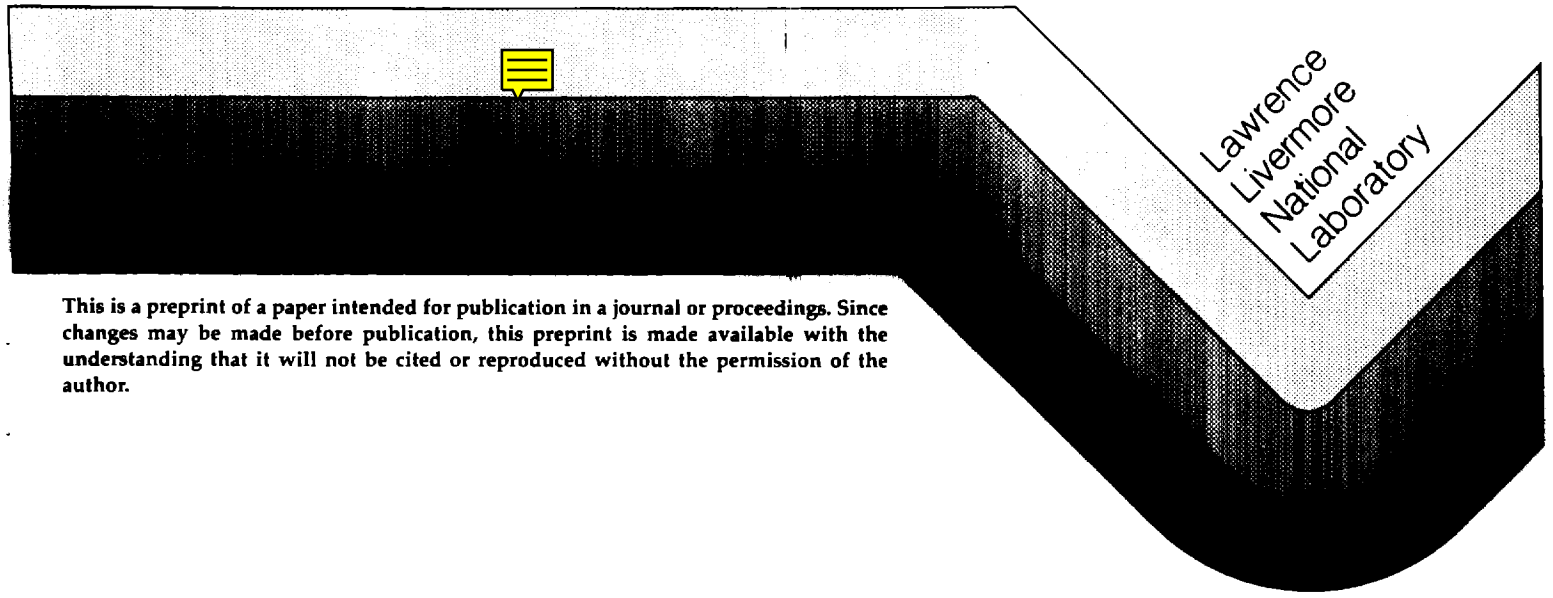

THE ASTROPHYSICAL JOURNAL, 277:296-311, 1984 February 1

A NUMERICAL STUDY OF NONSPHERICAL BLACK HOLE ACCRETION.* I. EQUATIONS AND TEST PROBLEMS

JOHN F. HAWLEY AND LARRY L. SMARR[1]
Department of Astronomy, University of Illinois

AND

JAMES R. WILSON
Lawrence Livermore National Laboratory
Received 1983 April 22; accepted 1983 June 20

ABSTRACT

We have developed a 2D axisymmetric, general relativistic code to study inviscid hydrodynamic accretion flows in a fixed Kerr black hole gravitational field. In this first of several papers documenting our methods and results, we describe and discuss the hydrodynamic equations in the form used in the code. Certain analytic solutions for shock tubes and special accretion flows are derived; these solutions will form the basis for code testing and calibration.

Subject headings: black holes — hydrodynamics — numerical methods — shock waves — stars: accretion

I. INTRODUCTION

There are a variety of astrophysical situations in which one expects to find fluid accreting onto a black hole. Among these are the stellar collapse to a black hole, a black hole in a binary system, and a supermassive black hole in an active galactic nucleus. In these situations, it is likely that the accreting matter will have angular momentum. In particular, a collapsing rotating star may leave behind considerable material with large angular momentum in a disk or ring around the newly formed black hole. For a black hole in a binary system, the matter is supplied by a companion which overfills its Roche lobe. The matter is then drawn into a ring or disk around the hole and is subsequently accreted. For supermassive holes, entire stars can supply mass for accretion. If a star ventures too close to such a hole, it can be tidally disrupted and left as a ring of high angular momentum matter orbiting the hole.

In each of these cases the subsequent accretion process is expected to proceed along the following general lines. Viscous or magnetic torques act to transport angular momentum outward, causing the bulk of the material to move inward, gaining internal energy at the expense of the gravitational field. This increase in energy and the resulting increase in pressure forces may cause the disk to grow outward from the equatorial plane, becoming a "fat disk" in which the vertical dimension of the disk is comparable with its radial size. Alternatively, the internal energy may be promptly radiated away, causing the disk to remain thin and roughly Keplerian. The differences in the observable features of these two types of flows can be quite significant.

While the processes of accretion onto a black hole have been described in very general terms, little is known of the specifics. Just what is the expected efficiency for each of the accretion scenarios? Are the most efficient processes likely to occur in astronomical regimes? Do stable accretion structures, such as fat disks, form in realistic flows? The consequences of the assumptions which go into these models have yet to be fully explored. A better understanding of black hole accretion will be required to describe the energy generation processes for quasars and jets. In addition, black hole detection may be made possible by determining what observational features are unique to black holes in binaries as opposed to other compact objects.

To study the process by which a fluid is accreted onto a black hole in complete generality, one must solve the equations of motion for the fluid and the Einstein equations (see, e.g., Smarr and Wilson 1983 or Evans 1983). The problem is greatly simplified by assuming that the total mass of accreting matter is small compared to the mass of the hole. One can then calculate the fluid dynamics in a fixed background metric. The problem is still *analytically* untenable unless one makes a series of very limiting assumptions. The use of a numerical computer code to solve the fluid equations allows us to be much less restrictive in seeking solutions to the dynamic fluid equations.

The study of the subsequent fluid flow in a Kerr metric after the collapse of a star was the motivation for the first such hydrodynamic accretion code (Wilson 1972). In this work, fat accretion disks were discovered numerically, demonstrating that even using inviscid hydrodynamics and a simple inflow with angular momentum, a complex structure involving shocks, circulation, and pressure support develops. This emphasizes the need for a greater understanding of the accretion process such as can only be achieved by examining solutions to the fluid equations obtained by numerical means.

Our goal is to develop an explicit Eulerian hydrodynamics code to be used as a research tool for studying fluid flow in axisymmetric stationary metrics. The code must be sufficiently "rugged" to allow easy adaptation to a wide variety of problems involving viscous heating, heat transport, energy loss by radiation, shocks, and other nonideal fluid phenomenon. In this paper we will discuss the numerical

[1] Alfred P. Sloan Fellow.

*This work was performed under the auspices of the U.S. Department of Energy by Lawrence Livermore National Laboratory under contract No. W-7405-Eng-48.

considerations only in the most general form. We shall concentrate on understanding the equations of hydrodynamics analytically in the form to be used in the code. Analytic solutions for fluid flow in the Kerr metric will be compiled and examined for use as code test problems. In our next paper we will describe various differencing schemes and discuss the results of the extensive finite difference and code testing which has been done.

II. DESCRIPTION OF EQUATIONS

a) *Variables, Coordinates, Units*

In this section both the fundamental and some derived variables are displayed as they will be used both in the code and in the analytic development below. Additional variables will be defined in § II*b* when they arise in context within the equations of hydrodynamics.

First consider the fluid variables. The fluid we wish to study will have a 4-velocity U^μ ($\mu = 0, 1, 2, 3$) at each point which is the 4-velocity of an observer comoving with the fluid at that point. Express the 4-velocity in units of the speed of light c. At this same point there are three scalar functions; the first of these is the baryon rest mass density $\rho(\text{g cm}^{-3})$. Consider only a one-particle fluid and allow no nuclear reactions. This allows the baryon mass density and the baryon number density (often written n by many authors) to be used interchangeably. The other scalar functions are the specific internal energy ϵ (ergs g^{-1})—the temperature in a perfect gas—and the isotropic pressure P (units of $\rho\epsilon$—energy density). The pressure P is connected to the other variables by an equation of state $P = P(\rho, \epsilon)$. We will often wish to consider the ideal gas equation of state given by $P = \rho\epsilon(\Gamma - 1)$, where Γ is the ideal gas adiabatic exponent. The relativistic enthalpy is written $h = 1 + \epsilon + P/\rho$. The quantity ρh is the total inertia-carrying mass energy. Note that for the ideal gas equations of state $\rho h = \rho(1 + \Gamma\epsilon)$. For a comparison of our notation to that of other authors, see Smarr, Taubes, and Wilson (1980).

We use geometric units in which $G = c = M = 1$ (M = black hole mass). To convert back to conventional units simply multiply the geometric value by dimensionally correct factors of G, c, and M. Note that since the mass of the accreting fluid does not contribute to the dynamics, the density is essentially scale-free. To describe an astrophysical problem in conventional units, relate the geometric density and energy to a referent value, such as the matter density and energy at infinity.

Next, let us define the important relativity variables. First the "relativistic gamma," often written γ, here written W:

$$W = (1 - V^\mu V_\mu)^{-1/2} . \tag{1a}$$

V^μ shall be referred to as the "transport velocity":

$$U^\mu = \frac{W}{\alpha} V^\mu . \tag{1b}$$

Next consider the "lapse function" $\alpha = (-g^{tt})^{-1/2}$. Proper time along the unit normal from one spacelike hypersurface at coordinate time t to a second such surface at coordinate time $t + dt$ is given by $d\tau = \alpha dt$. Together α and W make up respectively the total "gravitational" and "Doppler" redshift factor $W/\alpha = U^t$, the contravariant time component of the fluid 4-velocity.

Now consider the other components of the black hole metric g. The metric is assumed to be stationary and axisymmetric. It is completely specified by the mass of the hole M, and its angular momentum per unit mass a (Kerr geometry—assume charge Q on hole is zero). Express the metric in Schwarzschild-like (Boyer-Lindquist) coordinates. The line element is:

$$ds^2 = g_{tt}dt^2 + 2g_{t\phi}dtd\phi + g_{\phi\phi}d\phi^2 + g_{rr}dr^2 + g_{\theta\theta}d\theta^2 . \tag{2}$$

Choose the spacelike signature $(-, +, +, +)$.

The square root of the determinant of the four-metric is written $(-g)^{1/2}$. The square root of the determinant of the three-metric is written $\gamma^{1/2}$. The two are related by the lapse function:

$$\sqrt{-g} = \alpha\sqrt{\gamma} . \tag{3}$$

Use the usual forms for derivatives. The covariant derivative is signified by a semicolon or a "del" operator with a greek index; i.e.,

$$\nabla_\beta T^{\alpha\beta} = T^{\alpha\beta}{}_{;\beta} \tag{4}$$

signifies a covariant derivative with respect to β. Similarly, the ordinary flat-space derivative is signified with a comma or a latin index.

b) *Equations of Hydrodynamics*

The above variables give the complete state of a uniform-composition fluid system with no magnetic fields. Now assemble the equations which determine the evolution of such a fluid system. First there is the normalization of the 4-velocity:

$$U^\mu U_\mu = -1 . \tag{5}$$

Next there are two fundamental conservation laws. These are (1) the conservation of baryon number

$$\nabla^\mu(\rho U_\mu) = 0 , \tag{6}$$

and (2) the conservation of stress-energy

$$\nabla_\mu(T^{\mu\nu}) = 0 . \tag{7}$$

The tensor $T^{\mu\nu}$ is the stress-energy tensor to be discussed below. This second conservation law can be broken into two familiar forms: the conservation of energy

$$U^\mu\nabla^\nu T_{\mu\nu} = 0 , \tag{8}$$

and the conservation of momentum

$$h_{\gamma\mu}\nabla_\nu T^{\mu\nu} = 0 , \tag{9}$$

where $h_{\gamma\mu}$ is the spatial projection (into the fluid rest frame) tensor defined by

$$h_{\gamma\mu} = U_\gamma U_\mu + g_{\gamma\mu} . \tag{10}$$

The stress-energy tensor for an *imperfect* fluid is defined (Misner, Thorne, and Wheeler 1973; MTW) as

$$T^{\mu\nu} = \rho(1 + \epsilon)U^\mu U^\nu + (P - \zeta\theta)h^{\mu\nu} - 2\eta\sigma^{\mu\nu} + q^\mu U^\nu + q^\nu U^\mu . \tag{11}$$

The scalar functions η and ζ are the shear and bulk viscosities. The scalar θ is defined as

$$\theta = U^{\alpha}{}_{;\alpha} . \tag{12}$$

It describes the divergence or convergence of the fluid world lines. The symmetric, trace-free, and spatial shear tensor $\sigma^{\mu\nu}$ is defined by

$$\sigma^{\mu\nu} = \tfrac{1}{2}(U^{\mu}{}_{;\gamma} h^{\gamma\nu} + U^{\nu}{}_{;\gamma} h^{\gamma\mu}) - \tfrac{1}{3}\theta h^{\mu\nu} . \tag{13}$$

The vector q^{μ} is the energy flux vector.

These equations will describe the flow of an imperfect fluid for a fixed metric in complete generality. For the time being, consider an important subset of these equations, namely those describing a perfect fluid, by which is meant a fluid for which entropy is conserved along fluid lines. Entropy is changed in an imperfect fluid by viscosity and heat flow; exclude such terms from $T^{\mu\nu}$, leaving the perfect fluid stress-energy tensor:

$$T^{\mu\nu} = \rho h U^{\mu} U^{\nu} + P g^{\mu\nu} . \tag{14}$$

We now write the perfect fluid equations of hydrodynamics in the form in which they will be studied numerically (see, e.g., Wilson 1978). The law of baryon conservation can be written

$$\frac{1}{\sqrt{-g}} \partial_{\mu}(\rho \sqrt{-g}\, U^{\mu}) = 0 . \tag{15}$$

The metric is time independent by assumption. Now use the variable V^{μ} as defined in equation (1). This V^{μ} is the "transport velocity" of the fluid as measured by the observer at rest with respect to the coordinate grid points. Using this definition, write

$$\frac{1}{\sqrt{\gamma}} \partial_{\mu}(\rho \sqrt{\gamma}\, W V^{\mu}) = 0 . \tag{16}$$

Now define $D = \rho W$ and obtain

$$\partial_t(D) + \frac{1}{\sqrt{\gamma}} \partial_i(D \sqrt{\gamma}\, V^i) = 0 . \tag{17}$$

The energy equation is dealt with in a similar manner. Begin with

$$U^{\nu}[\nabla^{\mu}(\rho h U_{\mu} U_{\nu}) + \nabla_{\nu} P] = 0 . \tag{18}$$

Remove the term $\nabla^{\mu}(\rho U_{\mu})$ using baryon conservation; the remaining terms can be simplified to

$$\nabla^{\mu}(\rho \epsilon U_{\mu}) + P \nabla^{\mu} U_{\mu} = 0 . \tag{19}$$

Now define $E = \rho \epsilon W$ to obtain

$$\partial_t E + \frac{1}{\sqrt{\gamma}} \partial_i(E \sqrt{\gamma}\, V^i) + P \partial_t(W) + \frac{P}{\sqrt{\gamma}} \partial_i(W \sqrt{\gamma}\, V^i) = 0 . \tag{20}$$

For momentum conservation, take the divergence of the stress-energy

$$\nabla_{\mu}(\rho h U^{\mu} U_{\nu} + P g^{\mu}{}_{\nu}) = 0 \tag{21}$$

and use the definition $S_{\nu} = \rho h W U_{\nu}$ to write

$$\frac{1}{\alpha \sqrt{\gamma}} \partial_{\mu}(\sqrt{\gamma}\, S_{\nu} V^{\mu}) - \Gamma_{\mu\nu}{}^{\epsilon}\left(S_{\epsilon} \frac{V^{\mu}}{\alpha}\right) - \nabla_{\nu} P = 0 . \tag{22}$$

Note that $S^t = \rho h W U^t = \rho h W^2/\alpha$. Then

$$S_{\epsilon} V^{\mu}/\alpha = S_{\epsilon} S^{\mu}/\alpha S^t . \tag{23}$$

It is easily shown that

$$\Gamma_{\mu\nu}{}^{\gamma} S_{\gamma} S^{\mu} = \tfrac{1}{2} S^{\gamma} S^{\mu} \partial_{\nu} g_{\mu\gamma} = -\tfrac{1}{2} S_{\gamma} S_{\mu} \partial_{\nu} g^{\mu\gamma} . \tag{24}$$

After rewriting and taking the spatial component $\nu = j$, the momentum equation becomes

$$\partial_t(S_j) + \frac{1}{\sqrt{\gamma}} \partial_i(\sqrt{\gamma}\, S_j V^i) + \alpha \partial_j P + \frac{1}{2} \frac{S_{\gamma} S_{\mu}}{S^t} \partial_j g^{\gamma\mu} = 0 . \tag{25}$$

Our perfect fluid equations are now complete.

c) *Newtonian Limits*

The close relationship between the form of our equations of general relativistic hydrodynamics and the Newtonian hydrodynamics equations is made obvious by considering the Newtonian limit. In this limit we have:

$$U^{\mu} \to (1, V^i) , \quad W \to 1 , \quad h \to 1 , \quad D \to \rho , \quad E \to \rho\epsilon ,$$
$$S_{\mu} \to \rho U_{\mu} ,$$
$$\sqrt{\gamma} \to \text{flat space determinant (of the three-metric)} . \tag{26}$$

That is, we consider slow motions (relative to c), thermodynamically nonrelativistic (energy densities $\ll c^2$), in a weak gravitational field. The first two equations follow immediately: baryon conservation and energy conservation:

$$\partial_t \rho + \frac{1}{\sqrt{\gamma}} \partial_i(\rho \sqrt{\gamma}\, V^i) = 0 , \tag{27}$$

$$\partial_t(\rho\epsilon) + \frac{1}{\sqrt{\gamma}} \partial_i(\rho\epsilon \sqrt{\gamma}\, V^i) + \frac{P}{\sqrt{\gamma}} \partial_i(\sqrt{\gamma}\, V^i) = 0 . \tag{28}$$

For the momentum equation, first take the line element in the weak field limit as (MTW, eq. [16.2a])

$$ds^2 = -(1 + 2\Phi) dt^2 + (1 - 2\Phi) dr^2 + r^2 d\Omega^2 , \tag{29}$$

where Φ is the ordinary Newtonian potential. The Einstein equations reduce to $\Delta\Phi = 4\pi\rho$. Furthermore, the last term in the momentum equation becomes:

$$-\frac{1}{2} \frac{S^{\alpha} S^{\beta}}{S^t} \partial_j g_{\alpha\beta} = -\frac{1}{2} \rho(-2\partial_j \Phi) - \frac{1}{2}\left(\frac{V^r}{c}\right)^2 \rho(-2\partial_j \Phi)$$
$$\approx \rho \partial_j \Phi . \tag{30}$$

Additional accelerations, e.g., centrifugal, are also present in the derivative of the metric. For now, consider only the gravitational acceleration, i.e., neglect the terms involving U^{ϕ}, U^r, and U^{θ}. This weak field limit will be examined again in the discussion of stationary disks below (§ VI, eq. [81]). Using the gravitational acceleration, the momentum equation in the weak field limit is:

$$\partial_t(\rho V_j) + \frac{1}{\sqrt{\gamma}} \partial_i(\sqrt{\gamma}\, \rho V_j V^i) + \partial_i P + \rho \partial_j \Phi = 0 . \tag{31}$$

In the weak-field Newtonian limit the baryon conservation equation is recognized to be the usual continuity equation; the energy equation consists of transport of internal energy and the PdV work. The metric term in the momentum equation has revealed itself to be the gravitational acceleration. The close formal analogy between our equations and the usual Newtonian equations of hydrodynamics means that we can expect a similar analogy between the techniques developed to difference the Newtonian equations and the techniques to be used for the fully relativistic problem.

III. METHOD OF SOLUTION AND CODE DEVELOPMENT

a) Some General Code Features

We have listed the equations describing the fluid system; now we discuss the general philosophy and technique of the approach we use to numerically study this system. We wish to make clear the qualities desired in the code and the way in which these qualities are reflected in code strategy. This section is the first step in the complete documentation of our work. Such documentation is necessary not only to be able to properly interpret results, but also to take advantage of the new developments in numerical technique which may appear in the future.

Since we wish to study as wide a variety of physical systems as possible, the code must have sufficient generality and adaptability. Some of the fluid physics expected in accretion flows includes shocks, vortices, subsonic and supersonic flows, viscous effects, heating, cooling, angular momentum transport, and magnetic fields. The physics involved in such phenomenon is idealized and included in the differential equations through the addition of new terms, e.g., viscosity terms. When such terms are to be included in the difference equations, they should not require the development of an entirely new code. Rather, the new work should augment and build upon the old. Just as new physics is modeled by additional terms in the differential equations, we wish to include more physics by simply adding terms to the difference equations when possible.

Besides providing ease in applying new physics, a sufficiently adaptable code permits quick changes in finite difference methods. Not only does this allow for new or improved schemes to be immediately tested and used, but the comparison of results from schemes differing by only one technique or term is an excellent method of understanding exactly what features arise from the numerics and what represents physics.

These considerations require our two-dimensional (2D) code to be time-*explicit*; that is, each new time level is calculated using the values at the previous time level. The advantage of an explicit code is its simplicity. A time-*implicit* code involves obtaining the simultaneous solutions of all equations for the next time level. Further, the implicit difference equations are often difficult to formulate and code. In one spatial dimension, such codes are now in a state of mature development (e.g., Norman and Winkler 1983). However, in two spatial dimensions, such as we are studying, much more work and the use of supercomputers are required for time-implicit schemes.

An explicit code can use operator splitting (Wilson 1978) to solve one portion of the system of equations at a time. Finite difference methods are easily changed through the substitution of several lines of code; the whole program need not be rewritten. The major drawback to a time-explicit scheme is that it is Courant-Friedrichs-Lewy (CFL) limited; that is, the time step taken at each time level must be sufficiently small so that $\Delta t \leq \Delta x/c$, where Δx is the grid size and c is the local speed at which signals propagate through the grid. In fluid flows c is generally the sound speed. In relativistic problems c will be the speed of light since the function value obtain at each spacetime grid point is dependent on all the points in its backward facing light cone. Hence calculations involving long time scales (very many Δt) can be quite expensive to run; further, a decrease in the grid size (Δx) by a factor of 2 involves a corresponding decrease in time step and a total increase in run time by a factor of 8 (two factors of Δx because of two space dimensions; one factor of Δx from the CFL limit on Δt). Nevertheless, there are many problems which can be effectively investigated by an explicit code. Further, careful and extensive testing of explicit codes can lay the groundwork for future more accurate implicit codes.

We wish to study two-dimensional flows and such phenomena as vortices; the code must therefore be Eulerian, i.e., fixed grid, rather than Lagrangian in which the grid is tied to fluid elements. In more than one dimension, grid distortion and the tangling of grid lines make the Lagrangian scheme difficult to use. The main calculational difference between the Eulerian and the Lagrangian approach is that an Eulerian scheme must calculate the transport of fluid in and out of the fixed grid zones. By making these "transport" terms as accurate as possible, the disadvantages of the Eulerian scheme are minimized. Much space will be devoted to discussion and testing of finite difference transport schemes in the next paper in this series.

Shocks often play a key role in dynamic fluid flows. Such was the case in the first numerical study of 2D black hole accretion (Wilson 1972); and now, as then, we choose to employ an artificial viscosity Q to deal with shock discontinuities. An artificial viscosity has two functions to perform. One is to permit resolution of the shock on a finite difference grid by being sufficiently dissipative to spread the otherwise discontinuous shock over several grid zones. The other function is to model the conversion of kinetic energy into internal energy. Von Neumann and Richtmyer (1950) introduced a scalar Q which is added to the pressure in the stress-energy tensor; in this way it functions in the manner of a bulk viscosity term (see eq. [11]). We choose to use an artificial viscosity to handle shock discontinuities because of its generality. It does a quite adequate job of modeling shocks and it does not add significant numerical dissipation to the equations in regions away from shocks; it is set equal to zero unless there is local compression. In any case, all numerical schemes are inherently dissipative to some degree—one simply needs to understand and account for any effects which arise from unwanted numerical diffusion. Also important is that the use of Q is a general approach to the problem of shock dissipations, making it easier to eventually make use of an arbitrary equation of state and the inclusion of some form of dynamic viscosity. This will be necessary to study the transport of angular momentum and heating in accretion disks. In our second paper we will present extensive shock tube tests involving Q.

b) *Code Calibration*

In this section the philosophy of code testing and calibration is briefly discussed. Code development is a continuing process in which one maps out the desired equation-solving strategy, implements that strategy through coding, then compares results with intended goals by using checks for accuracy with known solutions, checks for self-consistency, and checks with physical intuition. Just as the experimental physicist must calibrate his laboratory equipment in order to interpret the results, the numerical theorist must similarly calibrate his code. This involves code testing. Such tests include studies of finite difference schemes in highly idealized, analytically clear-cut problems—e.g., shock tubes, advection of wave packets, simple accretion flows, etc. Particularly important are tests in the context of the problem one wishes to solve; in our case this means obtaining the special accretion flows which are analytically solvable. The goal of these tests is to gauge the magnitude of diffusive error inherent in the difference scheme, ensure self-consistency in the numerical formulation of the differential equations, demonstrate reproduction of analytic solutions, and check on the numerical simulation of each piece of physics as modeled by the equations.

We describe below the analytic solutions to a number of test problems both of a general nature and in the context of black hole accretion. In each case, the physical assumptions involved will be made explicit, the analytic solutions will be written down, and the specific aspects of the problem which make it suitable for code testing will be discussed.

IV. ONE-DIMENSIONAL SHOCK TUBES

a) *Newtonian Shock Problems*

We begin our discussion with the well known nonrelativistic test problem, the 1D Riemann shock tube. In this problem, hot dense gas on the left (fluid l) is separated by a membrane from cool, rarefied gas on the right (fluid r). At $t = 0$ the membrane is removed and fluid l pushes fluid r farther to the right, causing a rarefaction wave to move at the local sound speed back to the left through fluid l. The inflow of fluid l into fluid r causes a shock to travel to the right through fluid r. There are therefore five distinct regions in the flow (see Fig. 1). From left to right there is the undisturbed fluid l, the rarefaction wave, a region of constant velocity and pressure which features a contact discontinuity separating regions of different density, then the shock, and finally the undisturbed fluid r.

The analytic solution to this shock tube problem requires the use of (1) the characteristic curves of nonlinear waves and (2) conservation laws as realized in the shock jump conditions. The value of this problem as a code test also arises from these same features. It can test (1) how well a finite difference scheme advects a nonlinear wave and (2) if conserved quantities are actually conserved. It can also show how well the shock dissipation mechanism (e.g., artificial viscosity Q) provides the correct jump across the shock. A comparison of several finite difference schemes on the same problem is especially useful for displaying features in a solution which arise solely as a result of the numerics, e.g., the relative amounts of artificial dissipation and postshock oscillation (see, for example, Sod 1978).

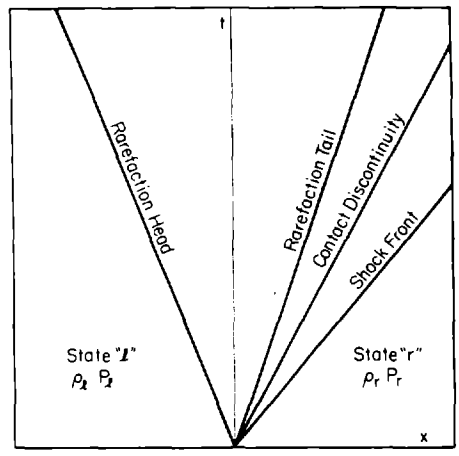

FIG. 1.—A spacetime diagram for the Riemann shock tube; the world lines show the location of the head and tail of the rarefaction wave, the contact discontinuity, and the shock. There are five distinct fluid states in the flow.

We briefly describe here the method for obtaining the analytic solution to the Riemann shock tube problem in Newtonian hydrodynamics. Although this solution is in the literature, it may not be familiar to some relativistic astrophysicists, so we outline the derivation here for completeness. A Newtonian flow is characterized by a specific internal energy much less than the rest mass energy, so our shock tube analysis will be valid only in cases in which the inequality $\epsilon \ll c^2$ holds. The solution presented here is from Courant and Friedrichs (1976), to which the reader is referred for a more complete discussion of shocks and related phenomena.

Consider the equation of baryon conservation in the 1D Newtonian limit:

$$\partial_t(\rho) + \partial_x(\rho V) = 0 , \tag{32}$$

and the momentum equation in the zero-field Newtonian limit:

$$\partial_t(\rho V) + \partial_x(\rho V \cdot V) + \partial_x P = \rho \partial_t V + \rho V \partial_x(V) + \partial_x P = 0 , \tag{33}$$

using baryon conservation.

This set of equations has two characteristic curves and two characteristic parameters. A characteristic curve of a set of differential equations is the locus of points along which some parameter of the problem, called a characteristic parameter, is constant. On these curves we may define a one-parameter ordinary differential equation (ODE); the set of both ODEs is equivalent to the original problem. For characteristic parameters α and β we have

$$\partial_\alpha V = -\frac{a_s}{\rho}\partial_\alpha \rho , \quad \partial_\beta V = \frac{a_s}{\rho}\partial_\beta \rho . \tag{34}$$

Note that for this set of nonlinear equations, the sound speed, a_s, is not a constant. Now assume that we have an isentropic flow, that is, for entropy s, $\nabla s = 0$ everywhere.

Then the characteristic equations can be integrated to yield

$$r(\beta) = \frac{V}{2} + \frac{\phi(\rho)}{2}, \quad \sigma(\alpha) = \frac{V}{2} - \frac{\phi(\rho)}{2}, \tag{35}$$

for

$$\phi(\rho) = \int_{\rho'}^{\rho} a_s \frac{d\rho}{\rho} = \int_{P'}^{P} \frac{dP}{a_s \rho}.$$

Assume $\phi = 0$ for $\rho' = 0$. The functions $r(\beta)$ and $\sigma(\alpha)$ are called the Riemann invariants of flow. Now further restrain the problem by assuming a polytropic equation of state, $P = K\rho^{\Gamma}$, and sound speed given by $a_s^2 = \Gamma P/\rho$. Then

$$\phi(\rho) = \frac{2}{\Gamma - 1} a_s = \frac{2}{\Gamma - 1} \sqrt{K\Gamma}\, \rho^{(\Gamma - 1)/2}, \tag{36}$$

and the Reimann invariants are

$$r = \frac{V}{2} + \frac{a_s}{\Gamma - 1} \text{ constant along } \frac{dx}{dt} = V + a_s, \tag{37a}$$

$$\sigma = \frac{V}{2} - \frac{a_s}{\Gamma - 1} \text{ constant along } \frac{dx}{dt} = V - a_s. \tag{37b}$$

These functions are constant along the appropriate characteristic. A fluid flow for which r or σ remains constant is called a simple wave. The rarefaction wave in our shock tube problem is such a simple wave; here σ is constant since the wave is moving backward through the grid, and the appropriate characteristic equation is equation (37b). Given an initial state V_0 and $(a_s)_0$, we may therefore write

$$V_0 - \frac{2}{\Gamma - 1}(a_s)_0 = V - \frac{2}{\Gamma - 1} a_s. \tag{38}$$

A simple wave starting from an initial state at rest at $x = 0$ is a centered simple wave; the characteristics all fan out in the (x, t)-plane from the origin. The rarefaction wave in the Riemann shock tube is a centered wave and as such it may be described by the equation $x = (V - a_s)t$. Consequently $V - a_s$ is a function of x/t, and the complete solution to the wave problem is therefore a function of the parameter x/t. Such a solution is called a similarity solution, and for a polytropic gas

$$a_s = \mu^2 \frac{x}{t} + (1 - \mu^2)(a_s)_0, \tag{39}$$

$$V = (1 - \mu^2)[x/t - (a_s)_0], \tag{40}$$

where $\mu^2 = (\Gamma - 1)/(\Gamma + 1)$. From this we can obtain ρ and P since $a_s = a_s(\rho)$ and $a_s = a_s(P)$ for a polytropic gas.

The solution for the shock must be obtained by different means. The shock is a discontinuity separating regions of constant velocity and density, V_1, ρ_1, to the right and V_2, ρ_2, to the left. Each of these regions is separately isentropic, but entropy s is discontinuous across the shock. In fact, by the second law of thermodynamics, the entropy must increase across the shock. Since the shock is inherently discontinuous, we must use conservation laws to relate the two states, 1 and 2. First, the mass flux into the shock must equal that leaving by the conservation of baryons. Similarly, momentum and energy flux must be conserved. For a shock front moving with velocity V_s we have the following jump conditions (Courant and Friedrichs 1976):

$$[\rho(V - V_s)] = 0, \tag{41a}$$

$$[\rho(V - V_s)^2 + P] = 0, \tag{41b}$$

$$[\rho(\tfrac{1}{2}V^2 + \epsilon)(V - V_s) + PV] = 0, \tag{41c}$$

with $[f] = f_+ - f_-$, where f_+ and f_- are the function f evaluated on either side of the shock discontinuity. Given the state on one side of a shock, the state on the other side is completely determined by the jump conditions and the specification of one additional value, e.g., shock speed V_s. In fact, for a polytropic gas, the specification of P_1 and V_1 in the preshock region yields a curve in the (P, V)-plane which describes the possible states P_2, V_2 behind the shock. Recall that since $a_s = a_s(P)$, a similar relationship may be constructed for the rarefaction wave.

To solve the Riemann shock tube, first obtain the curve of possible states for the rarefaction wave using the initial values of P_l and V_l in the hot dense region to the left of the membrane. Next obtain a similar curve for the shock using P, V in the cool region to the right. The intersection of these two curves yields the pressure and velocity in the intermediate region; this in turn determines the complete shock tube solution through the use of the rarefaction wave equations and the jump conditions.

To illustrate, we obtain the solution to the shock tube problem used by Sod (1978). First some discussion of units is in order so that the reader will be able to immediately compare our results to those of other authors. We take the units used in Sod's paper and show how the same shock problem can be posed in our units. In Sod's units the velocities are normalized to the sound speed; our velocities are normalized to the speed of light. Sod's initial conditions are $P_l = 1$, $\rho_l = 1$, $\epsilon_l = 2.5$, $V_l = 0$. and $P_r = 0.1$, $\rho_r = 0.125$, $\epsilon_r = 2$, and $V_r = 0$; the adiabatic exponent is equal to 1.4. Since a shock is characterized by the ratios across the shock in pressure, energy, and density, to convert to our units we need merely preserve these ratios while choosing values of P, ρ, and ϵ so as to ensure a Newtonian flow, $\epsilon \ll c^2$. One such set of values is $P_l = 1$, $\rho_l = 10^5$, $\epsilon_l = 2.5 \times 10^{-5}$, $V_l = 0$; $P_r = 0.1$, $\rho_r = 0.125 \times 10^5$, $\epsilon_r = 2 \times 10^{-5}$; $V_r = 0$. To convert Sod's velocities to our units, renormalize using the sound speed expressed in units where $c = 1$:

$$\frac{V_{\text{Sod}}}{(a_s)_{\text{Sod}}} = \frac{V}{a_s}. \tag{42}$$

We now set aside for the moment specific values and continue the analysis for initial states l and r. Given these states and using the jump conditions, we have for a shock wave moving to the right into fluid r an equation giving the velocity behind the shock as a function of V_r, P_r, and the postshock pressure P:

$$V = V_r + (P - P_r)\left[\frac{(1 - \mu^2)}{\rho_r(P + \mu^2 P_r)}\right]^{1/2}. \tag{43}$$

This equation is the curve in the (P, V)-plane which describes the possible postshock states. The rarefaction wave moving to the left is described by the equation $V - a_s = V_l - (a_s)_l$. Substituting in the polytropic equations for a_s and

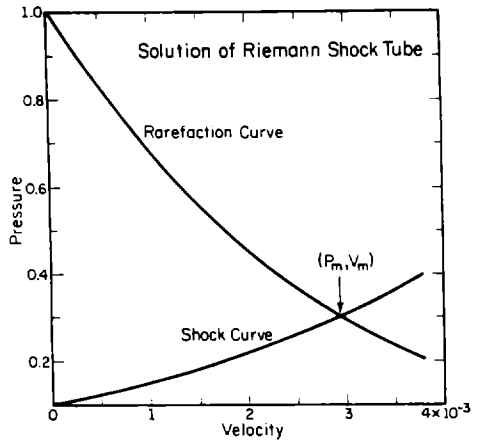

FIG. 2.—Curves in the (P, V)-plane, one describing possible fluid states in the rarefaction wave and the other the possible postshock states. The intersection of the two curves is the solution for the intermediate state in the shock tube problem.

expressing velocity as a function of pressure, we get

$$V = V_l - \frac{(1-\mu^4)^{1/2}}{\mu^2}\frac{P_l^{1/(2\Gamma)}}{\rho_l^{1/2}}\left(P^{(\Gamma-1)/2\Gamma} - P_l^{(\Gamma-1)/2\Gamma}\right). \quad (44)$$

This is also a curve in the (P, V)-plane, here describing the possible values of P and V in the rarefaction wave. The intersection of these two curves gives the value of pressure and velocity in the intermediate region, P_m and V_m, which connect the right moving shock with the left moving rarefaction wave. For our problem, $V_l = V_r = 0$ and we may write:

$$V_m = (P_m - P_r)\left[\frac{(1-\mu^2)^2}{\rho_r(P_m + \mu^2 P_r)}\right]^{1/2}. \quad (45)$$

For the particular values of P and ρ given above we obtain $P_m = 0.303$ and hence $V_m = 2.93 \times 10^{-3}$ (see Fig. 2).

Having obtained the pressure and velocity of the intermediate state m, calculate the remaining hydrodynamic values. First obtain the postshock density by combining the jump conditions to obtain

$$\frac{\rho_2}{\rho_1} = \left(\frac{\Gamma+1}{\Gamma-1}\frac{P_2}{P_1} + 1\right)\Big/\left(\frac{\Gamma+1}{\Gamma-1} + \frac{P_2}{P_1}\right). \quad (46)$$

For this problem, $\rho_2 = 0.266 \times 10^5$.

The solution for the contact discontinuity is especially simple. It moves from its initial position at the membrane at $t = 0$ to the right at velocity V_m. Behind the contact is the region described by the rarefaction wave equation. Expressing this equation in terms of P and ρ, we obtain

$$\rho = \rho_m\left[1 + \frac{\Gamma-1}{2}\left(\frac{V - V_m}{(a_s)_m}\right)\right]^{2/(\Gamma-1)},$$
$$P = P_m\left[1 + \frac{\Gamma-1}{2}\left(\frac{V - V_m}{(a_s)_m}\right)\right]^{2\Gamma/(\Gamma-1)}. \quad (47)$$

These equations yield the solution for ρ and P in the wave back to the undisturbed region at the left. The value ρ_m is obtained from the polytrope relation $\rho_m = \rho_l(P_m/P_l)^{1/\Gamma}$. For this example $\rho_m = 0.426 \times 10^5$. This completes the solution to the Riemann shock tube problem and the results are displayed graphically in Figure 3.

b) *Relativistic Shock Problems*

Relax the assumption that the specific internal energy must be small, $\epsilon \ll c^2$, and allow non-Newtonian hydrodynamic flows. In the 1D special-relativistic zero field limit, the equations of baryon, energy, and momentum conservation become

$$\partial_t(D) + \partial_x(DV) = 0, \quad (48)$$
$$\partial_t(E) + \partial_x(EV) + P\partial_t W + P\partial_x(VW) = 0, \quad (49)$$
$$\partial_t S + \partial_x(SV) + \partial_x P = 0. \quad (50)$$

The variables used here are the same as defined above in § II*a*. V is again the coordinate velocity related to the fluid 4-velocity by $U^\mu = W(1, V^i)$ $(\alpha = 1)$.

The advantage of having special relativistic shock problems in the test ensemble is that, in conjunction with the nonrelativistic problems, they allow isolation and testing of the specifically relativistic terms. These include the renormalization of the 4-velocity, calculation of V and W, the pressure terms in the energy equation which involve W, and the role of artificial viscosity Q in special-relativistic flows. The goal of these tests is to single out and examine the unique numerical difficulties which arise from these terms.

As in the nonrelativistic case, a Riemann shock tube problem may be formulated and a solution obtained. The procedure is exactly analogous to that described above except that the relativistic Riemann invariants and jump conditions must be used; they are derived by Taub (1948), and their consequences and some solutions are investigated by Johnson and McKee (1971), Eltgroth (1971), and Thorne (1973). The relativistic shock tube is one of the problems used in our code testing; specific solutions are obtained by Centralla and Wilson (1983). We confine the present discussion to the qualitative differences between the relativistic and the nonrelativistic shock tube.

For the relativistic 1D flow, Taub obtains the relativistic Riemann invariants (compare eq. [35]):

$$r = \phi + \ln\left(\frac{1+V}{1-V}\right)^{1/2}, \quad \sigma = \phi - \ln\left(\frac{1+V}{1-V}\right)^{1/2}, \quad (51)$$

where r is constant along the curve

$$dx/dt = (a_s + V)/(1 + a_s V) \quad (52)$$

and σ is constant along

$$dx/dt = (a_s - V)/(1 - a_s V). \quad (53)$$

Here a_s is the relativistic sound speed defined by

$$a_s^{\rm rel} = d\ln(\rho h)/d\ln(\rho). \quad (54)$$

In the equations for the characteristic curves, the previous Galilean sum or difference of sound speed and fluid velocity (eqs. [37a, b]) has been replaced by the relativistic sum or difference. Similarly, the quantity ϕ is defined as before except that the sound speed is relativistic and the density is replaced with the total energy density in the pressure formulation:

$$\phi = \int \frac{a_s}{\rho}\,d\rho = \int \frac{dP}{a_s \rho h}. \quad (55)$$

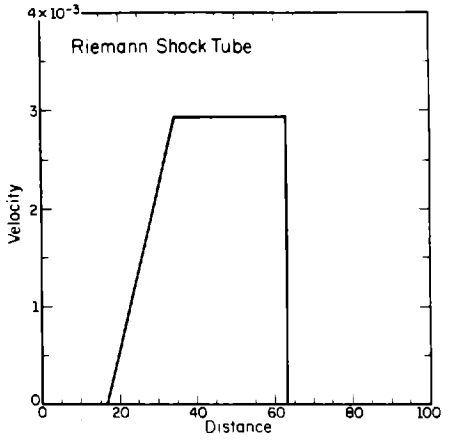

FIG. 3a

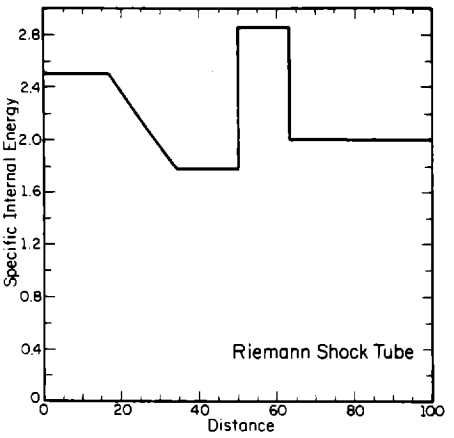

FIG. 3c

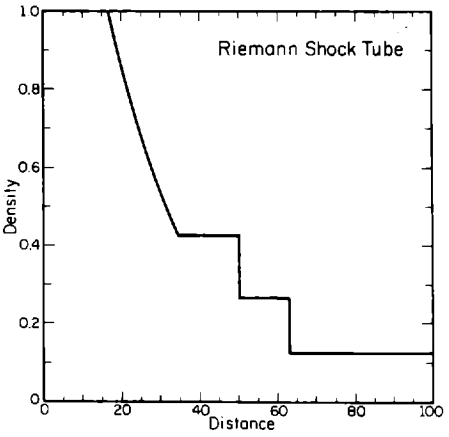

FIG. 3b

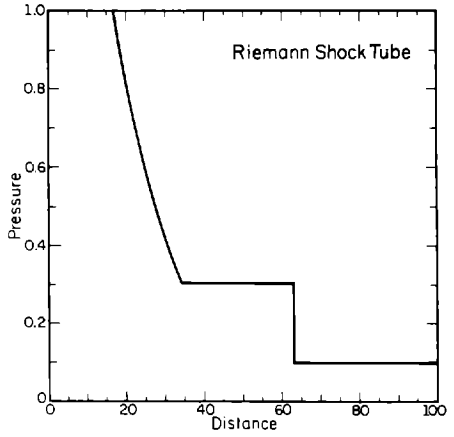

FIG. 3d

FIG. 3.—Solution to the nonrelativistic shock tube problem at $t = 5000$ for (*a*) velocity, (*b*) density, (*c*) specific internal energy, and (*d*) pressure. The spatial location of the shock and contact are $x_s = 63.1$, $x_c = 50.1$; the rarefaction wave runs from $x = 16.7$ to 34.1.

The relativistic jump conditions are also just the relativistic generalization of the Newtonian conditions already discussed. In the frame in which the shock is at rest we have (Thorne 1973):

$$[\rho WV] = 0\,, \tag{56a}$$

$$[\rho hWV^2 + P] = 0\,, \tag{56b}$$

$$[\rho hWV] = 0\,. \tag{56c}$$

The use of these jump conditions is greatly simplified by neglecting the preshock pressure, often a very good assumption in the relativistic shock.

An example of a special relativistic Riemann shock tube solution is shown in Figure 4. The pictured problem is a $\Gamma = 5/3$ gas with $D = 10.0$, $E = 20.0$ ($\epsilon = 2$) on the left and $D = 1$, $E = 10^{-6}$ on the right. The intermediate pressure and velocity are $P_m = 1.384$, $V_m = 0.69$, $W_m = 1.38$ (mildly relativistic). Density $D(=\rho W) = 3.55$ at the end of the rarefaction wave, and $D = 6.85$ in the postshock region. Note that the velocity is no longer linear in the rarefaction region; this is a consequence of the relativistic velocity addition. The shocked region in fluid r becomes narrower in width because of Lorentz contraction; the apparent difference between shock velocity V_s and the intermediate velocity V_m in the laboratory frame becomes smaller as both values approach c. The jump in density across the shock is larger than predicted for a Newtonian shock. Taking the limit of negligible preshock internal energy, the laboratory frame jump conditions predict a compression ratio

$$\frac{\rho_2}{\rho_1} = \frac{\Gamma + 1}{\Gamma - 1} + \frac{\Gamma}{\Gamma - 1}(W_m - 1)\,. \tag{57}$$

The ratio $(\Gamma + 1)/(\Gamma - 1)$ is the maximum expected from Newtonian theory. The shock velocity in the frame of the unshocked fluid (here the laboratory frame) is given by

$$V_s = \left\{\frac{1 + [\Gamma/(\Gamma - 1)](W_m V_m)^2}{\rho_1 + [\Gamma/(\Gamma - 1)]W_m P_m}\right\}\frac{P_m}{W_m V_m}\,. \tag{58}$$

As in the nonrelativistic case, the relativistic shock tube allows testing of nonlinear wave advection and conservation laws. In the relativistic case, it is particularly useful to single out for study the shock jump conditions in a second test problem. For this problem the initial conditions consist of cold

matter at constant density ρ_1 with a relativistic velocity V_1. This fluid is run into a reflecting boundary (wall) at one end of the grid. This causes a shock to form which then moves back through the grid, leaving behind hot, dense material with zero velocity in the postshock region. In this problem the jump conditions alone determine the state behind the shock, ρ_2, ϵ_2. The compression ratio is the same as that given in equation (57). The specific internal energy can be determined from the jump conditions or by simply equating kinetic energy per nucleon in the preshock region with internal energy per nucleon behind the shock:

$$W(1 + \epsilon_1) = 1 + \epsilon_2 . \tag{59}$$

For our wall shock problem, we have taken the limit $\epsilon_1 = 0$, consequently $\epsilon_2 = W - 1$. The shock velocity is obtained from the jump conditions:

$$V_s = V_1 \Big/ \left(\frac{\rho_2}{\rho_1} \frac{1}{W} - 1 \right) . \tag{60}$$

A typical example of this type of problem is given in Figure 5. In this example we consider a $\Gamma = 4/3$ gas with initial conditions $V_1 = 0.832$, $D_1 = 1$ ($\rho_1 = 0.556$), $W = 1.80$; the postshock values are $D_2 = \rho_2 = 5.67$, $E = 4.57$ ($\epsilon = 0.80$).

V. RADIAL ACCRETION ONTO BLACK HOLES

Now consider the analytic solutions for specific accretion flows onto black holes. These solutions are obtainable by making a set of quite restrictive assumptions which greatly simplify the differential equations. They are excellent for code testing since each represents a specific limit of the general physical problem for which the code was designed.

The first analytic solutions considered are those for steady-state radial accretion of an ideal fluid onto a Kerr black hole. Consider the fluid evolution equations; use the assumptions "steady state" and "radial" to eliminate all partial derivatives except ∂_r. Then the density and energy equations are

$$\partial_r(DV^r\sqrt{\gamma}) = 0 , \tag{61}$$

$$\partial_r(EV^r\sqrt{\gamma}) + P\partial_r(W\sqrt{\gamma}\,V^r) = 0 . \tag{62}$$

Since the metric is known and fixed, and $U_\phi = U_\theta = 0$, knowledge of $V^r(r)$ yields a solution for $D(r)$ and $E(r)$. $V^r(r)$

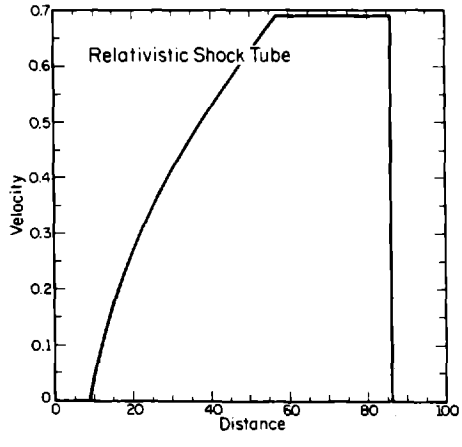

FIG. 4a

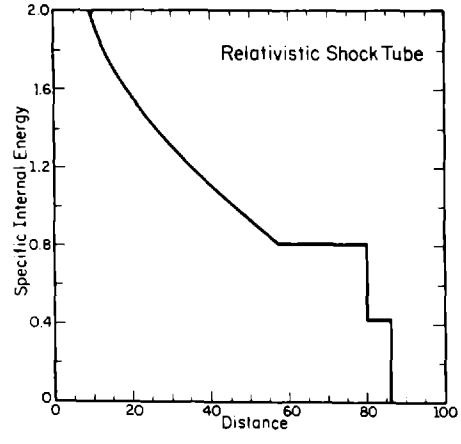

FIG. 4c

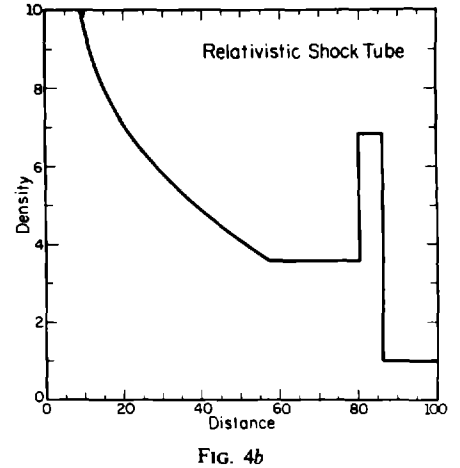

FIG. 4b

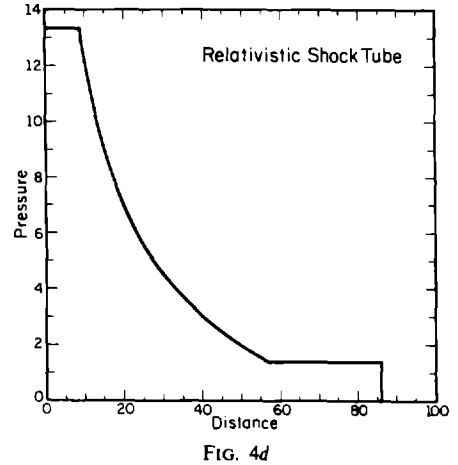

FIG. 4d

FIG. 4.—Solution to the relativistic shock tube problem for (*a*) velocity, (*b*) density, (*c*) specific internal energy, and (*d*) pressure. The spatial location of the shock and contact are $x_s = 86.3$, $x_c = 80.0$; the rarefaction wave runs from $x = 8.0$ to $x = 57.0$.

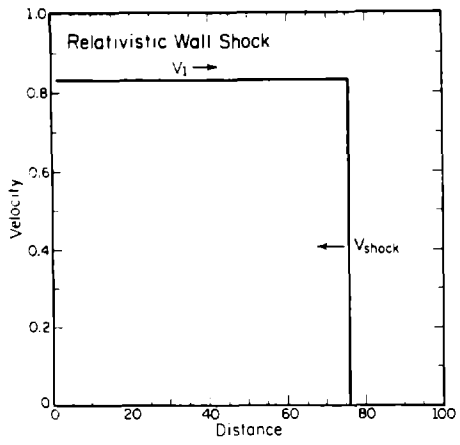

FIG. 5a

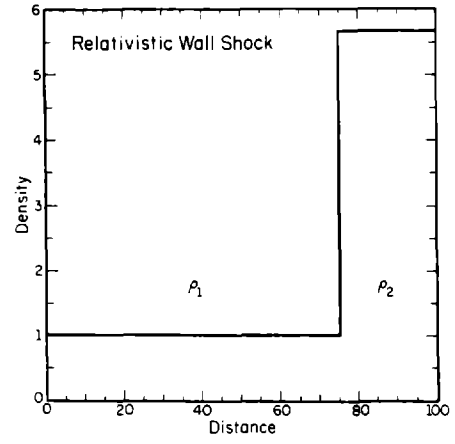

FIG. 5b

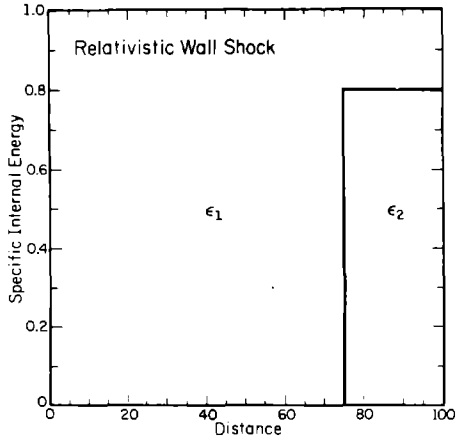

FIG. 5c

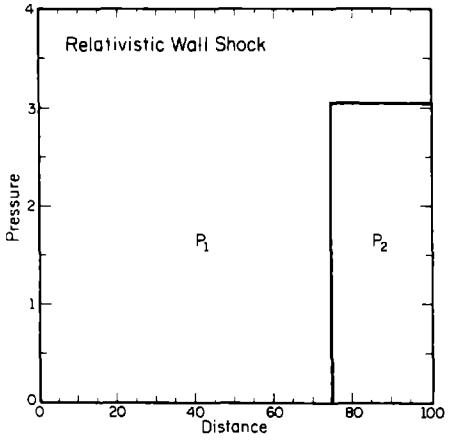

FIG. 5d

FIG. 5.—Solution to the relativistic "wall shock" problem for (*a*) velocity, (*b*) density, and (*c*) specific internal energy. The spatial location of the shock is $x_s = 75$. The shock is moving to the left with velocity $V_{shock} = 0.178$.

is in general obtained from the momentum evolution equation; here, however, it is obtained directly as a consequence of restrictive assumptions. We study two such restrictions: (1) the case of radial accretion with negligible pressure ("geodesic flow"), and (2) the Bondi radial flow solution with a sonic point.

a) Geodesic Flow

First we consider the radial accretion of noninteracting test fluid particles or "dust." The assumption is that the elements of the accreting fluid fall along geodesics. In axisymmetric, steady-state flows the binding energy per baryon hU_t is conserved. Hence for dust particles, the gravitational binding energy U_t will remain constant. Since $U^\mu U_\mu = -1$, $V^r(r)$ is now determined in terms of the input constant U_t and the known metric functions. In general, for $U_\theta = U_\phi = 0$,

$$V^r = \frac{U^r}{U^t} = \frac{g^{rr}}{g^{tt}U_t}\left(\frac{-1 - g^{tt}U_t^2}{g^{rr}}\right)^{1/2} . \tag{63}$$

Free-falling fluid particles are by definition noninteracting. This means that the fluid pressure force must be entirely negligible and the ratio $E/D = \epsilon = P/[\rho(\Gamma - 1)]$ must be much less than one. Note that since $P = 0$ is not required, the PdV terms in the energy equation, while negligible in determining the function $V^r(r)$, can still be important in determining $E(r)$ and should be retained.

We now have a one-parameter (U_t) family of solutions of the hydrodynamic equations for a given Kerr (a/M) hole with the restriction $E/D \ll 1$. To explicitly exhibit the solution, we use equation (63) to get $V^r(r)$. With $V^r(r)$ known, the density equation can be immediately integrated:

$$DV^r\sqrt{\gamma} = \text{constant} = d . \tag{64}$$

To integrate the energy equation, rewrite it as the sum of three exact differentials:

$$\frac{1}{E}\partial_r E + \frac{1}{V^r\sqrt{\gamma}}\partial_r(V^r\sqrt{\gamma}) + \frac{(\Gamma - 1)}{V^r\sqrt{\gamma}\,W}\partial_r(W\sqrt{\gamma}\,V^r)$$
$$= \partial_r \ln E + \partial_r \ln (V^r\sqrt{\gamma}) + (\Gamma - 1)\partial_r \ln (\sqrt{\gamma}\,V^r W) = 0 . \tag{65}$$

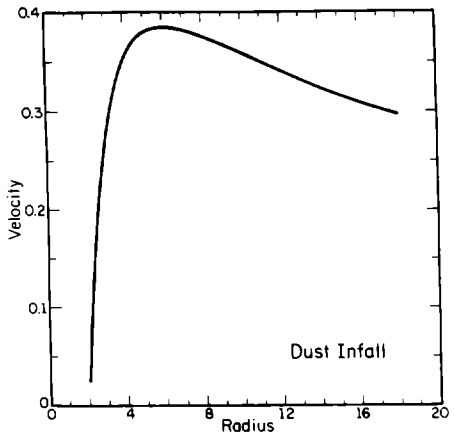

FIG. 6a

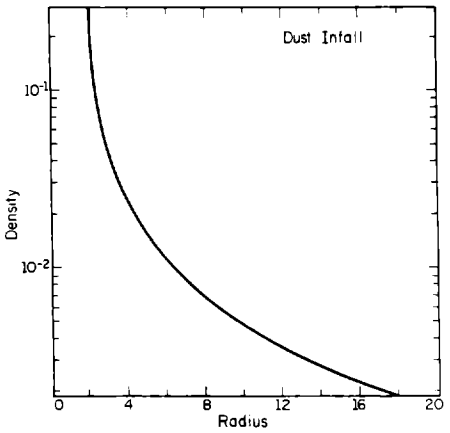

FIG. 6b

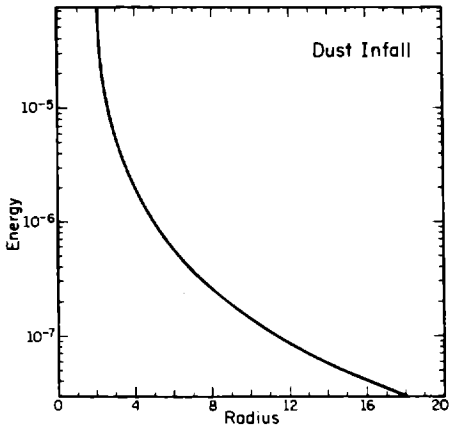

FIG. 6c

FIG. 6.—Function $V(r)$, $D(r)$, and $E(r)$ for the radial infall of marginally bound dust. The radius is measured in units of M and the velocity in units of c. The energy is normalized to the value $E = 10^{-7}$ at the test grid outer boundary $r = 11.3$. The density is normalized by setting the mass flux equal to the mass flux in the transonic inflow problem shown in Fig. 7.

This equation is valid for an ideal gas $[P = (\Gamma - 1)E/W]$ with a constant binding energy U_t $(U^t = 1/\alpha^2|U_t|)$. Now rewrite and integrate to obtain:

$$E = \frac{e\alpha^{\Gamma-1}}{(\sqrt{\gamma}\,V^r)^\Gamma}, \tag{66}$$

where e is the constant of integration.

We now present a particular solution of this one-parameter family for a Schwarzschild black hole: the marginally bound case $U_t = -1$. In this simplest example we can analytically solve for $D(r)$, $E(r)$, and $V^r(r)$ as:

$$D(r) = d/\{r^2[(2m/r)(1 - 2m/r)]^{1/2}\}, \tag{67a}$$

$$E(r) = e/[(\sqrt{2m/r}\,r^2)^\Gamma(1 - 2m/r)^{(\Gamma+1)/4}], \tag{67b}$$

$$V(r) = \sqrt{2m/r}\,(1 - 2m/r), \tag{67c}$$

$$S(r) = [D(r) + \Gamma E(r)]\sqrt{2m/r}/(1 - 2m/r). \tag{67d}$$

The functions $V^r(r)$, $D(r)$, and $E(r)$ are shown in Figure 6. Several features of these functions are common to all accretion problems. First while the proper velocity U^r approaches c as r approaches $2m$, the coordinate velocity V^r goes to zero due to the "redshift factor" U^t (time dilation). At the same time the functions D and E are diverging, again due to the same redshift factor. Here the same number of baryons is found in an increasingly smaller coordinate volume as r approaches $2m$.

As a test problem the radial infall of dust involves checks on the radial transport terms, geometric terms, and the general-relativistic redshift factors, velocity normalization, and to a lesser extent the pressure terms in the energy equation. More importantly, this problem provides an excellent way of exploring code dynamics in a very noncomplicated context; the problem is run as an approach to a steady state analytic solution rather than simple maintenance of that solution. This test involves for the first time the outer grid boundary and the horizon as an inner boundary in the same type of grid and with the same code on which more complex problems will later be run.

b) *Sonic Point Flow*

Now drop the assumption of geodesic motion everywhere and allow E to be of the same order as D. The analytic solution to the equation is now the generalization of the Bondi accretion problem to the Schwarzschild metric. This problem has been investigated in detail (Michel 1972; Begelman 1978; Ray 1980) for the case of an equation of state given by the ideal gas law $P = \rho\epsilon(\Gamma - 1)$. Other investigators have solved the radial accretion problem in astrophysical contexts, including additional effects such as radiation transport, more general equations of state, and magnetic effects (Shapiro 1973*a*, *b*, 1974; Blumenthal and Mathews 1976; Mézáros 1975). The most complete study of spherical accretion into black holes is presented in a series of papers by Thorne, Flammang, and Żytkow (1981) and Flammang (1982, 1983).

Following Michel, we define $T = P/\rho = (\Gamma - 1)\epsilon$ and write the law of baryon conservation in the form

$$T^n U^r r^2 = C_1, \tag{68}$$

where n is the polytropic index $[=1/(\Gamma-1)]$ and U^r is the radial component of the four velocity U^μ, for which $U^\mu U_\mu = -1$. Next the energy flux equation $T^\mu{}_{r;\mu} = 0$ is written in the form:

$$[1 + (1+n)T]^2[1 - 2m/r + (U^r)^2] = C_2 . \tag{69}$$

These two equations will determine the two unknowns U^r and T at each r provided the constants C_1 and C_2 are known. Michel obtains these constants by considering the asymptotic limit to obtain C_2 in terms of T_∞ and by using the "critical point" analysis to determine C_1. This analysis involves differentiating equations (68) and (69) to obtain (for $u = U^r$)

$$0 = \frac{du}{u}\left[V_s^2 - \frac{u^2}{(1 - 2m/r + u^2)}\right] + \frac{dr}{r}\left[2V_s^2 - \frac{m}{r(1 - 2m/r + u^2)}\right] \tag{70}$$

with sound speed

$$V_s^2 = \frac{d \ln (P + \rho + \rho\epsilon)}{d \ln \rho} - 1 .$$

The critical point occurs where the factors in the brackets vanish, i.e., when

$$u_c^2 = m/2r_c , \tag{71}$$

$$V_c^2 = u_c^2/(1 - 3u_c^2) . \tag{72}$$

This is the Schwarzschild generalization of the Bondi critical point (Bondi 1952) which simply states that given an accretion rate, the flow must go from a subsonic to a supersonic regime at a specific radius r_c, which is determined entirely by the constants of the motion, if the flow is to be continuous, smooth, and steady state. Here we see this expressed as the statement that a given choice of constants C_1 and C_2 yields a unique solution for $u(r)$ and $T(r)$.

Rather than obtain a solution in terms of asymptotic thermodynamic values, we select instead a desired value of r_c. This then determines u_c and T_c through the equations

$$u_c^2 = \frac{m}{2r_c} , \tag{73}$$

$$\frac{(1+n)T_c}{n[1 + (1+n)T_c]} = V_c^2 = \frac{u_c^2}{(1 - 3u_c^2)} . \tag{74}$$

Thus the choice of r_c in equations (71) and (72) selects both C_1 and C_2 determining a unique set $u(r)$ and $T(r)$. $T(r)$ is obtained by writing

$$u(r) = C_1/T^n r^2 , \tag{75}$$

$$[1 + (1+n)T]^2\left(1 - \frac{2m}{r} + \frac{C_1^2}{r^4 T^{2n}}\right) = C_2 . \tag{76}$$

For $\Gamma = 5/3$ this yields a fifth order polynomial for T. Having obtained a solution for $T(r)$ and $u(r)$, we can then obtain the value of each code variable. First

$$\frac{\rho}{\rho_\infty} = \left(\frac{T}{T_\infty}\right)^n ; \tag{77}$$

hence

$$\rho = (\rho_\infty/T_\infty{}^n)T^n = KT^n . \tag{78}$$

The constant K determines the adiabat. Here for simplicity choose $K = 1$. Next

$$T = \frac{P}{\rho} = \frac{\rho\epsilon(\Gamma - 1)}{\rho} = \frac{E(\Gamma - 1)}{D} , \tag{79}$$

where

$$D = \rho U^t \alpha \quad \text{and} \quad E = \rho\epsilon U^t \alpha ;$$

and since

$$\rho U^r r^2 = C_1 , \quad D = \frac{C_1 U^t \alpha}{(U^r r^2)} , \tag{80}$$

U^t is obtained using the normalization of the 4-velocity.

Figure 7 shows the functions $V^r(r)$, $D(r)$, and $E(r)$. Note in particular that V^r is reduced below its free-fall value by the pressure support the now hot ($E \sim D$) gas provides.

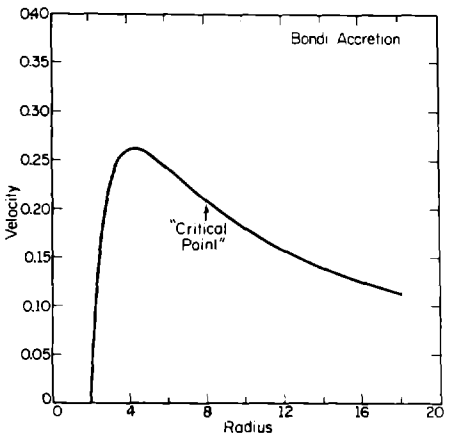

FIG. 7a

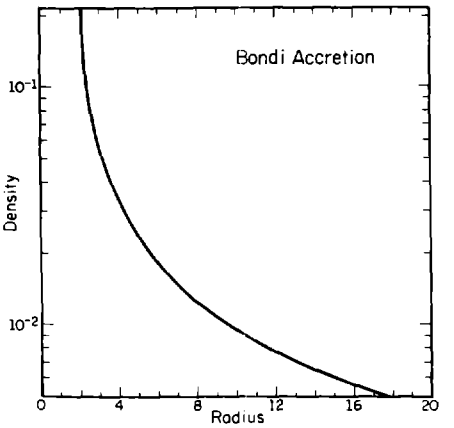

FIG. 7b

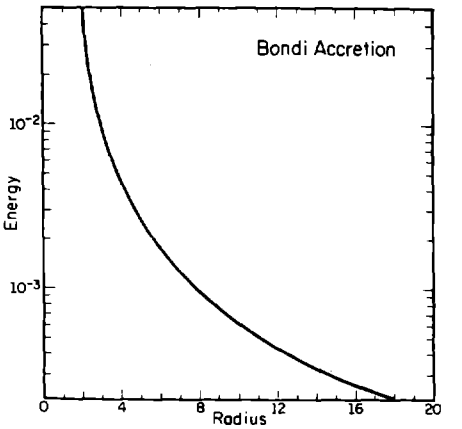

FIG. 7c

FIG. 7.—Functions $V(r)$, $D(r)$, and $E(r)$ for radial transonic inflow of fluid with nonzero pressure

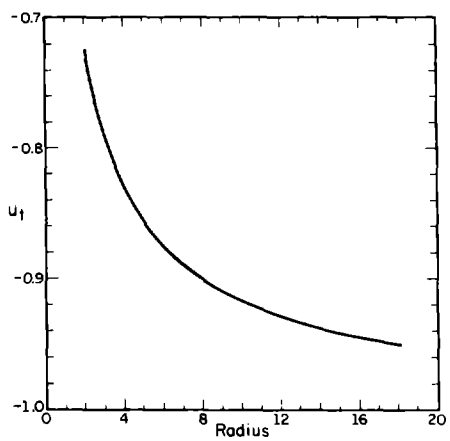

FIG. 8.—Four-velocity component U_i vs. radius for transonic inflow. For adiabatic, time-stationary flows hU_t is conserved, thus U_t is constant (geodesic motion) only when $\epsilon + P/\rho \ll c^2$.

Figure 8 is the function $U_t(r)$. In the geodesic case this function was constant. Here it increases monotonically from its asymptotic value of ~ -1. Marginally bound fluid with significant pressure is heated by compression as it falls at the expense of the gravitational field. Note that this shows that even in a supersonic flow such as this it is not necessarily a good assumption to consider the fluid to be free-falling. The validity of that assumption is determined by the ratio of E/D, that is, by the relative importance of pressure forces.

The sonic point flow provides the same code checks as dust infall plus more stringently testing the role of the pressure terms in determining the flow; in particular the pressure acceleration term is now important. The inner and outer boundaries must also be handled in a more general fashion. However, the most important feature of this test problem is the demonstration of the code's ability to find the sonic point in an accretion flow. The location of the sonic point is an issue of some importance in general flows, for example in the case of fat accretion disks (see Liang and Thompson 1980; Abramowicz and Zurek 1981).

VI. TWO-DIMENSIONAL ACCRETION FLOWS—FAT DISKS

Since the accretion flows to be studied will in general involve angular momentum, these flows will be two-dimensional, often with U^θ on the same order as U^r. It would therefore be valuable to have a 2D test ensemble as well as a radial one. Unfortunately, 2D flows are not easily solvable by analytic means. However there is an analytically described 2D structure which can be adopted as a test problem. This is the pressure-balanced fat disk.

We now review the theory of stationary fat disks, but done in our variables. There are essentially three accelerations per unit mass acting upon the fluid: pressure gradients, gravitational accelerations and centripetal acceleration. Referring back to the momentum evolution equation (eq. [25]), we see that in a stationary model the time derivative and transport terms vanish. The term ∇P is the pressure gradient; therefore, the last term involving gradients of the metric must hide the gravitational and centripetal acceleration terms. To see where they are hidden, we take the weak-field Newtonian limit of this latter term.

For the stationary model in the weak field Newtonian limit we can extend our earlier analysis (eq. [29]) to include the angular momentum:

$$\frac{\partial_i P}{\rho} = \frac{1}{2}\partial_i(2\Phi) - \frac{1}{2}(U_\phi)^2\partial_i g^{\phi\phi} = \partial_i\Phi - \frac{1}{2}(U_\phi)^2\partial_i\left(\frac{1}{R^2}\right), \tag{81}$$

where R is the distance from the axis of rotation (cylindrical coordinates). Thus we have obtained the usual Newtonian equations for hydrostatic equilibrium of a fluid with angular momentum U_ϕ in a potential Φ:

$$\frac{\partial P}{\partial R} = \rho\left(\frac{\partial\Phi}{\partial R} + \frac{U_\phi{}^2}{R^3}\right), \quad \frac{\partial P}{\partial Z} = \rho\frac{\partial\Phi}{\partial Z}. \tag{82}$$

The solution of these equations will yield a stationary fat disk structure in which the gravitational, centrifugal, and pressure gradient forces are all in balance. This weak-field analysis highlights the essential physics, but in what follows all our work will be fully relativistic.

Such a relativistic disk structure was discovered numerically by Wilson (1972) in his dynamical study of fluid flow in Kerr space. He found that cold material with high angular momentum falling toward a Kerr hole was not immediately accreted; rather, a hot shock region (fat disk) formed (see his Figs. 2*g* and 2*h*). The standing shock at the outer boundary of the disk slowly grew outward as material continuously fell through it. In addition a circulation current was established behind the shock, driven by the entropy gradient across the shock. Thus, this was a quasi-stationary fat disk with U_r, U_θ, and U_ϕ all nonzero. This rather complicated structure showed for the first time that stationary fat disks around black holes can form.

Later investigators discussed the fat disk analytically. Rotating fat disks with no internal motion ($U_r = U_\theta = 0$) were described analytically by Fishbone and Moncrief (1976), by Abramowicz, Jaroszyński, and Sikora (1977, AJS), and by Kozłowski, Jaroszyński, and Abramowicz (1977, KJA). Lynden-Bell (1977) emphasized the natural presence of "funnels" (the boundary of the fat disk) along the hole axis in general relativity. These provide a means to produce and collimate relativistic jets generated near the hole. He showed that one can find analytically the shape of this funnel for a stationary fat disk. Here we rework these authors' results in terms of our variables.

Consider a perfect fluid in a known stationary axisymmetric metric $g^{\mu\nu}$ in which we neglect the self-gravity of the fluid. The conventional way to yield the balance of pressure gradients, gravitational acceleration, and centripetal acceleration is to assume the flow is purely azimuthal and stationary and to use the relativistic Euler equation (see, e.g., Smarr, Taubes, and Wilson 1980, eq. [19]) written in the rest frame of the fluid:

$$\rho h a_i = \nabla_i P, \tag{83}$$

to derive the equation of force balance. This is straightforward since in the case of no internal motion we can write:

$$U_\mu = U_t(1, 0, 0, -l), \tag{84a}$$

$$U^\mu = U^t(1, 0, 0, \Omega), \tag{84b}$$

with $U^\mu U_\mu = -1$ yielding U_t as a function of l and Ω:

$$U^2{}_t = -(g_{t\phi}{}^2 - g_{tt}g_{\phi\phi})/(g_{\phi\phi} + 2lg_{t\phi} + l^2 g_{tt}) . \quad (85)$$

Here l is the angular momentum per unit mass defined to be $-U_\phi/U_t$ and Ω is the angular velocity defined as U^ϕ/U^t. As KJA point out, such definitions have the advantage over the use of U_ϕ as the specific angular momentum since l is conserved along streamlines for this 4-velocity whereas U_ϕ is conserved only for the case of dust, as was previously pointed out. The separately conserved quantities are hU_t and hU_ϕ. Now using the definition of the 4-acceleration,

$$a_\mu = U^\nu \nabla_\nu U_\mu , \quad (86)$$

we find the master force balance equation to be

$$\frac{\nabla_i P}{\rho h} = -\nabla_i \ln(-U_t) + \frac{\Omega \nabla_i l}{1 - \Omega l} , \quad (87)$$

which is the same as equation (7) of AJS.

However, our code can find much more general time-dependent flows with internal motion (U_r and U_θ nonzero). Our time-dependent Euler equations (eq. [25]) reduce to their simple analytic result for the case of time-independent azimuthal-only flow:

$$\nabla_i P = -\tfrac{1}{2}\partial_i g^{\alpha\beta} S_\alpha S_\beta / S^t \quad (88)$$

(since $\partial_t S_i = V^i = 0$, $i = r, \theta$). This is the strong field version of the weak field limit given above (eq. [81]). One can see how the more general flows with U_r, U_θ nonzero naturally emerge from our time-dependent equations.

Von Zeipel's theorem is a powerful tool for understanding such flows. In a general flow where $P = P(\rho, \epsilon)$, such as our code can handle, the surfaces of constant l and constant Ω do not coincide. If the equation of state is simplified to a barotropic one, i.e., dependent only upon the total mass-energy, $P = P(\rho + \rho\epsilon)$, then the constant-$l$ and constant-Ω surfaces coincide (see Abramowicz 1974; Seguin 1975). If one chooses the particular barotropic condition $\nabla s = 0$, i.e., isentropic, then these level surfaces of constant l and Ω also coincide with surfaces of constant hU_ϕ, the conserved angular momentum per baryon. This latter very special case is the one which is obtained when one writes the equation of state as $P = K\rho^\Gamma$, where $\nabla s = 0$.

The result that the surfaces of constant l and Ω coincide for an equation of state $P = P(\rho + \rho\epsilon)$ allows AJS to solve equation (87), writing

$$\int_0^P \frac{dP}{\rho h} = -\ln(-U_t) + \ln(-U_t)_{\rm in} + F(l) , \quad (89)$$

where

$$F(l) = \int_{l_{\rm in}}^{l} \frac{\Omega dl}{1 - \Omega l} .$$

The subscript "in" refers to the inner boundary of the disk. By requiring the equation of state to be barotropic, von Zeipel's theorem guarantees that all our quantities of interest will be functions of one variable, here the variable l.

The total potential Ψ is defined as

$$\Psi - \Psi_{\rm in} = \ln(-U_t) - \ln(-U_t)_{\rm in} - \int_{l_{\rm in}}^{l} \frac{\Omega dl}{1 - \Omega l} . \quad (90)$$

Thus, the specification of the function $\Omega(l)$ completely specifies the model, given an equation of state $P(\rho + \rho\epsilon)$. Note, however, that the model will not be physical wherever the lines of constant potential Ψ are open onto the hole. In such an instance U^r cannot be equal to zero and material will flow into the hole. The same is true in the case where the potential lines are open to infinity except that the fluid will then be unbound. Thus, the analytic formulation gives the solution in only part of space—inside the closed potentials of the fat disk. To obtain the fluid flow in all of space, one must also cover the unbound areas where the analytic formalism breaks down. This is why a numerical study of these fat disks is very fruitful even in the stationary fat disk case.

We now choose some very specific models out of the collection described by equation (89). First we choose, as do AJS, to model disks with constant specific angular momentum, that is, l = constant. This implies $F(l) = 0$, so we can simplify equation (89):

$$\int_0^P \frac{dP}{\rho h} = -\ln(-U_t) + \ln(-U_t)_{\rm in} . \quad (91)$$

Physically, such a rotation law represents a vortex with the angular velocity becoming arbitrarily large near the axis.

Next we choose a polytropic equation of state, $P = K\rho^\Gamma$. If we require K to be constant throughout the entire disk, then an isentropic model is obtained. This is a great simplification and will definitely not hold in a realistic, dynamic flow; in such flows entropy gradients and shocks can play a major role in establishing circulations like the kind observed by Wilson (1972). Here, however, this assumption simplifies the integration of the left-hand side of equation (91). Using the first law in the form

$$0 = Tds = dh - dP/\rho , \quad (92)$$

we find

$$\int_0^P \frac{dP}{\rho h} = \ln(h) - \ln(h)_{\rm in} , \quad (93)$$

where h is the enthalpy. We may then equate $\ln(-U_t) = -\ln(h)$.

The code uses an ideal gas equation of state with $P = \rho\epsilon(\Gamma - 1)$ which is more general than the polytropic form assumed here in the initial conditions. To construct a model in terms of our code variables from their U_t, write

$$\epsilon = \frac{1}{\Gamma}\left(-\frac{1}{U_t} - 1\right) . \quad (94a)$$

Since

$$P = \rho\epsilon(\Gamma - 1) = K\rho^\Gamma , \quad (94b)$$

then

$$\rho = \left[\frac{\epsilon(\Gamma - 1)}{K}\right]^{1/(\Gamma - 1)} , \quad (94c)$$

where K is arbitrary. Thus for

$$U_t(r, \theta) = -(|g^{tt} - 2lg^{t\phi} + l^2 g^{\phi\phi}|)^{-1/2} \quad (95a)$$

we have

$$D(r, \theta) = \left[\frac{\epsilon(r, \theta)(\Gamma - 1)}{K}\right]^{1/(\Gamma-1)} W(r, \theta), \quad (95b)$$

$$E(r, \theta) = \epsilon(r, \theta) D(r, \theta) W(r, \theta), \quad (95c)$$

$$S_\phi(r, \theta) = (D + \Gamma E)(-l) U_t(r, \theta), \quad (95d)$$

with

$$W(r, \theta) = \alpha U^t(r, \theta), \quad (95e)$$

using equation (94a) for $E(r, \theta)$.

Now specification of K and l determines a model. The analytic value of each code variable at each grid point is determined from these equations, and those data are used as the initial conditions for the code. In addition we require that in the region where $U_t < -1$, U_t be equal to -1 and D and E be some negligible value. This simplifies the models so that we study only the bound disk structure. The model of a fat, pressure-supported disk can now be evolved.

The evolution has two major goals. First, it should test the code by seeing how stationary the matter remains in the bound region. Second, it will find the actual flow lines of the matter (U_r, $U_\phi \neq 0$) when there are unbound regions (open potential lines) and the analytic method is useless. We have chosen three models which represent the three types of solutions one obtains, namely (1) the specific angular momentum is less than that of the marginally stable Keplerian orbit, $l < l_{ms}$ (see AJS); no fluid element has sufficient angular momentum to prevent accretion onto the hole; (2) the specific angular momentum is sufficient to keep some but not all of the bound fluid ($U_t > -1.0$) off the hole, $l < l_{ms}$, but less than the angular momentum of the Keplerian marginally bound orbit, l_{mb}; and (3) the specific angular momentum is sufficiently large that all the bound fluid is supported off the hole, $l > l_{mb}$. Analytic density plots for these three examples are shown in Figure 9.

In the first case above, with constant angular momentum $l < l_{ms}$, while there is no analytic solution for the fluid inflow which will result, one qualitatively expects certain features. The fluid should "drain" out of the disk smoothly; initially when the infall velocity is small, l should remain constant and the potentials should maintain the same shape. The fluid infall velocity vectors should be perpendicular to the local potential. Finally the equidensity contours should continue to coincide with the equipotentials.

The second case, $l_{ms} < l < l_{mb}$, is similar to the first in that there will be dynamic flow. However, here a portion of the fluid will have sufficient angular momentum to remain orbiting the hole. Further, all accretion into the hole will be constrained to flow through the narrow spout at the potential cusp.

The third case, $l > l_{mb}$, is especially simple: U_r and U_θ should remain zero and l constant. This is a steady state problem in which a delicate balance between pressure, gravitational, and centrifugal forces must be maintained.

These test problems employ the full 2D nature of the code; angular boundary conditions, 2D operator splitting, and angular momentum transport are involved for the first time. Also these cases provide the opportunity to investigate numerical diffusion. Such diffusion leads to the artificial smoothing out of a distribution, e.g., a density function, on a finite difference grid. One case in particular is the artificial separation of angular momentum and density caused by numerical diffusion (see Norman, Wilson, and Barton 1980) for a discussion of this problem and its role in the study of

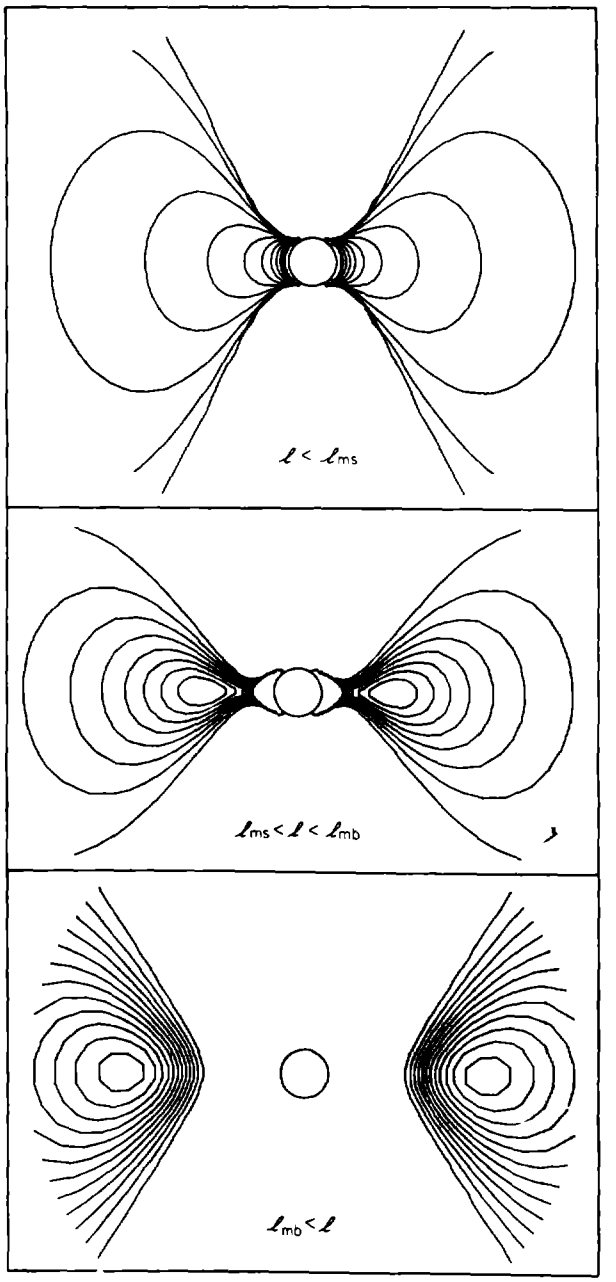

FIG. 9.—Density plots for constant angular momentum fat disks orbiting a black hole. These models were obtained by assuming that $U_r = U_\theta = 0$. Three cases are illustrated: (*a*) $l < l_{ms}$, (*b*) $l_{ms} < l < l_{mb}$, (*c*) $l > l_{mb}$ (see text). These curves are generated from initial conditions on a finite-difference grid, and consequently some discretization error is present. Most apparent are the "pincers" on the hole in case *b*. The analytic curves actually merge onto the hole axis.

2D protostar collapse). The role of these tests, in particular the steady state models, is in part to investigate these phenomena for various finite difference schemes. Stationary models with large gradients in angular momentum are also quite useful. They can be easily constructed by specifying some function l along the equator, with $\partial_R l \geq 0$ (stability criterion, see Seguin 1975), and solving for the potential.

VII. CONCLUSIONS

We have presented a systematic development of the general-relativistic equations of hydrodynamics as we will difference them. Some analytic solutions to these equations have been derived so as to provide a complete background against which to develop and calibrate our 2D code. These exact problems will be numerically solved in our next paper, providing both code testing and comparison of several numerical methods.

Partial support for this work was provided by the National Science Foundation through grant PHY 80-01496 and by the Department of Energy. The National Center for Atmospheric Research is acknowledged as the source for the graphics software. Computational work was performed on the University of Illinois Cyber 175 and the VAX and Image Processing System, operated jointly by the Departments of Astronomy and Atmospheric Science and the Computer Services Office. One of us (J. H.) wishes to thank Martin Rees and Mitch Begelman for enlightening discussions and the Institute of Astronomy, Cambridge, UK, for its hospitality. Finally we thank Joan Centrella, Mike Norman, and K.-H. Winkler for many illuminating discussions on code differencing and testing.

REFERENCES

Abramowicz, M. A. 1974, *Acta Astr.*, **24**, 45.
Abramowicz, M., Jaroszyński, M., and Sikora, M. 1978, *Astr. Ap.*, **63**, 221 (AJS).
Abramowicz, M. A., and Zurek, W. H. 1981, *Ap. J.*, **246**, 314.
Begelman, M. C. 1978, *Astr. Ap.*, **70**, 583.
Blumenthal, G. R., and Mathews, W. E. 1976, *Ap. J.*, **203**, 714.
Bondi, H. 1952, *M.N.R.A.S.*, **112**, 195.
Centrella, J., and Wilson, J. R. 1983, *Ap. J.*, **273**, 428.
Courant, R., and Friedrichs, K. O. 1976, *Supersonic Flow and Shock Waves* (New York: Springer-Verlag).
Eltgroth, P. G. 1971, *Phys. Fluids*, **14**, 2631.
Evans, C. 1983, in *Numerical Astrophysics: A Festschrift in Honor of James R. Wilson*, ed. J. Centrella, R. Bowers, J. LeBlanc, M. LeBlanc (Portola Valley: Jones and Bartlet), in press.
Fishbone, L. G., and Moncrief, V. 1976, *Ap. J.*, **207**, 926.
Flammang, R. A. 1982, *M.N.R.A.S.*, **199**, 833.
———. 1983, *M.N.R.A.S.*, in preparation.
Johnson, M. H., and McKee, C. F. 1971, *Phys. Rev. D*, **3**, 858.
Kozłowski, M., Jaroszyński, M., and Abramowicz, M. A. 1978, *Astr. Ap.*, **63**, 209 (KJA).
Liang, E. P. T., and Thompson, K. A. 1980, *Ap. J.*, **240**, 271.
Lynden-Bell, D. 1977, *Phys. Scripta*, **17**, 185.
Mészáros, P. 1975, *Astr. Ap.*, **44**, 59.
Michel, F. C. 1972, *Ap. Space Sci.*, **15**, 153.
Misner, C., Thorne, K., and Wheeler, J. 1973, *Gravitation* (San Francisco: Freeman) (MTW).
Norman, M. L., Wilson, J. R., and Barton, R. T. 1980, *Ap. J.*, **239**, 968.
Norman, M. L., and Winkler, K.-H. 1983, in *Radiation Hydrodynamics*, ed. M. Norman and K.-H. Winkler (Dordrecht: Reidel), in press.
Ray, D. 1980, *Astr. Ap.*, **82**, 368.
Seguin, F. 1975, *Ap. J.*, **197**, 745.
Shapiro, S. L. 1973*a*, *Ap. J.*, **180**, 531.
———. 1973*b*, *Ap. J.*, **185**, 69.
———. 1974, *Ap. J.*, **189**, 343.
Smarr, L. L., Taubs, C., and Wilson, J. R. 1980, from *Essays in General Relativity*, ed. F. J. Tipler (New York: Academic Press).
Smarr, L. L., and Wilson, J. R. 1983, in *Radiation Hydrodynamics*, ed. M. Norman and K.-H. Winkler (Dordrecht: Reidel), in press.
Sod, G. A. 1978, *J. Comp. Phys.*, **27**, 1.
Taub, A. 1948, *Phys. Rev.*, **74**, 328.
Thorne, K. S. 1973, *Ap. J.*, **179**, 897.
Thorne, K. S., Flammang, R. A., and Żytkow, A. N. 1981, *M.N.R.A.S.*, **194**, 475.
Von Neumann, J., and Richtmyer, R. D. 1950, *J. Appl. Phys.*, **21**, 232.
Wilson, J. R. 1972, *Ap. J.*, **173**, 431.
———. 1978, in *Proceedings of Int. Sch. of Phys. Fermi Course LXV* (Amsterdam: North-Holland).

JOHN F. HAWLEY and LARRY L. SMARR: University of Illinois, Astronomy Department, 341 Astronomy Building, 1011 W. Springfield Ave., Urbana, IL 61801-3000

JAMES R. WILSON: L-35, Lawrence Livermore National Laboratory, Livermore, CA 94550